Julia Kundin, Hedieh Farhandi, Kamatchi Priya Ganesan, Renato S. M. Almeida, Kamen Tushtev, Kurosch Rezwan

Phase-field modeling of grain growth in presence of grain boundary diffusion and segregation in ceramic matrix mini-composites

Journal Article as: peer-reviewed accepted version (Postprint)

DOI of this document*(secondary publication): 10.26092/elib/2607

Publication date of this document: 20/10/2023

* for better findability or for reliable citation

Recommended Citation (primary publication/Version of Record) incl. DOI:

Julia Kundin, Hedieh Farhandi, Kamatchi Priya Ganesan, Renato S.M. Almeida, Kamen Tushtev, Kurosch Rezwan, Phase-field modeling of grain growth in presence of grain boundary diffusion and segregation in ceramic matrix mini-composites,
Computational Materials Science, Volume 190, 2021, 110295, ISSN 0927-0256,
https://doi.org/10.1016/j.commatsci.2021.110295.

Phase-field modeling of grain growth in presence of grain boundary diffusion and segregation in ceramic matrix mini-composites

Julia Kundin [a,*], Hedieh Farhandi [b], Kamatchi Priya Ganesan [c], Renato S.M. Almeida [b], Kamen Tushtev [b], Kurosch Rezwan [b,d]

[a] ICAMS, Ruhr-University Bochum, D-44801 Bochum, Germany
[b] Advanced Ceramics, Univesity Bremen, D-28359 Bremen, Germany
[c] Indian Institute of Technology Madras, 600036, India
[d] MAPEX-Center for Materials and Processes, University of Bremen, D-28359 Bremen, Germany

Keywords:
Grain growth
Grain boundary diffusion
Phase-field modeling
Ceramic Matrix Composites
Ceramic fibers
Nextel 610

A B S T R A C T

The grain boundary diffusion and segregation can influence the grain growth kinetics, the grain size distribution, and therefore the mechanical properties of the ceramic matrix composites. The present paper proposes a phase-field modeling approach to simulate the grain growth in polycrystalline alumina fibers embedded in alumina matrix at temperatures above 1000 C in presence of the grain boundary diffusion of dopants from the matrix to the fiber and vice versa. The multi-phase-field model for grain growth [I. Steinbach and F. Pezzolla, Phys. D, 134 (1999) 385] is extended by the incorporation of the grain boundary diffusion, grain boundary segregation model, and the dependence of the interface mobility on the segregation concentration. The kinetic parameters of the model which allow describing the real microstructure evolution were estimated by the comparison to the experimental measurements.

The simulation and experimental results of the grain growth with the diffusion of dopants in Nextel 610 fibers show the significant effect of the grain boundary diffusion on the grain size distribution. The results of numerical tests were used to adjust the values of the grain boundary diffusion coefficients by the experimental data at different temperatures by means of an inverse method. From the simulations, the diffusion coefficient of Mg was estimated to be 6 7 times higher than that of Si.

1. Introduction

Since the mechanical properties of oxide ceramic matrix composites (Ox-CMCs) are mostly dependent on the strength of the oxide fibers which are used as the reinforcement [1], many studies have investigated the effect of high temperature on fiber degradation [1 5]. Although comparatively, the brittle matrix has significantly lower strength [6], the adjustment of the matrix composition can influence the microstructural and subsequently mechanical performance of the composites.

Schmücker et al. [2] showed that the fine-grained fiber microstructure of Nextel 610 is more prone to coarsening when the fibers are in contact with alumina-based ceramic matrix. Moreover, it was found that pronounced grain growth occurs predominantly in the peripheral zone of the fibers in comparison to the fibers center [1 3]. This observation was explained in terms of outwards diffusion of silica, which is normally added as dopants to reduce the grain boundary (GB) mobility of the fibers. Electron beam microprobe analysis of the spatial elemental distribution of Si clearly indicates this diffusion effect, resulting in a concentration profile with maximum Si content in the fiber center and gradually decreasing towards fiber periphery and matrix [2]. However, the precise temperature where the silica diffusion start to influence of grain growth is still unknown. In order to avoid the outwards diffusion of Si, the composition of the matrix can be adjusted to reduce chemical composition gradient between fiber and matrix [1]. A more recent study [7] on the changes of the grain structure for Nextel 610 fibers embedded in mullite-SiOC matrix confirms the previous results, although an opposite effect was observed. The original grain size was found to be retained only in a small stripe at the periphery of the fibers while the grain growth occurs in the center of the fibers. This fact could be explained by similar diffusion effects, but in this case, an inwards diffusion of matrix constituents into the fibers could be expected. Besides silica, the presence of Y and La cations at the interface reduce the

* Corresponding author.
E-mail address: julia.kundin@ruhr-uni-bochum.de (J. Kundin).

GB energy and make the GB more stable [8]. The studies of the sintering and grain growth in alumina ceramics showed that MgO doping has an inhibition effect on the grain growth [9,10].

The influence of additives and segregation on the kinetics of the grain growth was investigated in ceramics theoretically and experimentally in many works. To get a fine grain size, additives/dopants are added to render the grain growth by decreasing its GB energy or GB mobility. Weissmüller et al. first formulated their thermodynamic treatment based on Gibbs adsorption equation for decreasing GB energy by segregation on grain boundaries [11]. Later a number of theoretical works were carried out to develop this approach and a good agreement with related experimental results was found [12 15]. Kirchheim and Liu [13] proved the McLean s grain boundary model [16] by experiments that the segregation decreases the GB mobility and inhibits grain growth. Aidhy et al.[17] elucidate a framework using atomistic simulations of ceria to design dopant-pinned grain boundaries that prevent the grain growth. Gong et al. [18] showed that the retardation of grain growth in nanocrystalline ceramics is caused by the reduced GB energy and the reduced GB mobility which are dopant-segregation-dependent. Furthermore, increased GB segregation enthalpy and decreased GB diffusion coefficient of dopant cation in lanthana-doped alumina leads to a promoted sintering behavior in a alumina system, i.e., a higher relative density at the same grain size [19].

Dillon et al. [20,21] performed an extensive kinetic study of grain-boundary transport kinetics in alumina for a number of dopant chemistries over a broad temperature range. The data show that the grain-boundary mobilities are proportional to grain-boundary diffusivities. There was found the remarkable correlation between grain-boundary complexion and grain growth kinetics. In the review papers [22 24] the different complexion in alumina and their effect on the normal and abnormal grain growth are widely discussed. The diffusion in polycrystalline materials follows the different mechanisms: (i) volume diffusion through inner region of the crystal or the bulk diffusion; (ii) grain boundary diffusion through interfaces of the polycrystals which are disordered, and (iii) surface diffusion, which can occur both in single crystals and polycrystals. In polycrystalline material the grain boundary diffusion is faster than the bulk diffusion [25]. Grain boundary (GB) diffusion plays an important role in many processes taking place in engineering materials at elevated temperatures. Such processes include creep, sintering, diffusion-induced grain boundary migration, discontinuous reactions (such as discontinuous precipitation, discontinuous coarsening, etc.), recrystallization, and grain growth.

The model for a semi-infinite diffusion system was initially developed by Fisher [26] and the analytical solutions were obtained by Whipple and Suzuoka [27,29]. Fisher initially considered differences in diffusivity between grain boundary and the bulk crystal. He assumed that along the grain boundary the diffusivity are higher than in the bulk. Additionally, there is no flux between grain boundary and the bulk material. Whipple obtained the analytical solution for the same physical model by considering the flux distribution between grain boundary and bulk material. Later, Sozuoka [28] used the same Fisher s model to derive his equation for a thin film where the tracer atoms are deposited on the surface of the sample. In all three model variants, the authors consider the large bulk crystal and a small diffusion time across the grain boundary [30]. Later Gilmer and Farrell [31,32] and Preis and Sitte [33] developed a new model for thin films of finite thickness. In this model they embedded the highly diffusive slab in between two plane surfaces. The model was analysed by Hwang and Balluffi [34] and applied to polycrystalline thin films. Further, Bokshtein et al. [35] developed spherical grain model which was used by Preis [36] for thin films. This model has spherical grains enclosed in the squares as grain boundaries. Belova and Murch [37] modeled the 2D polycrystals as the square grains separated by straight lines as grain boundaries by the similar approach. Levine and MacCallum [38] considered grains as randomly oriented polyhedra of different size. Recently, Chen and Schuh [39] extended these approaches and suggested to consider the polycrystal as a binary composite of grains and intergranular regions including the dual boundaries and triple junctions.

Table 1
Average grain size, *d*, standard error, average feret, and maximum feret diameters of fibers alone (as-received) and fibers embedded in alumina matrix with and without dopants obtained for experimental SEM images of the microstructure after 2 h of heat treatment. All sizes are in nm.

Conditions	Position	Av. size	St. error	Av. feret	Max. feret
As-received	center	87	1.1	88	120
1200 C, no dopant	rim	97	1.4	98	198
1200 C, with MgO	rim	84	1.1	99	200
1300 C, no dopant	rim	173	5.5	277	1040
1300 C, with MgO	rim	133	3.4	185	801
1400 C, no dopant	rim	298	5.9	775	1986
1400 C, with MgO	rim	229	5.6	602	1374

The influence of segregation of matrix and fiber dopants (MgO and SiO_2) on the grain growth and the grain size distribution in alumina and mullite-based fibers are studied in the present work by phase-field modeling. A phase-field model which takes into account the reduction in GB mobility during segregation on grain boundaries was recently suggested by the authors [40]. In this work, we will extend the multi-phase-field approach to the GB diffusion of two species between the matrix and the fiber. Our purpose is to describe the changes in the microstructure of the fibers during the heat treatment process which are influenced by inwards and outwards diffusion in matrix and fiber components. Since the interface in the phase-field approach is diffuse, the flux between the grain boundary and the bulk is incorporated naturally. The phase-field model which we will apply in this study is an efficient approach to simulate the ideal grain growth first suggested by Steinbach et al. [41]. The modeling approach related to the present study are, e.q., the works of Steinbach, Song and Hartmaier [42] and Kamachali et al. [43] where the grain growth with the elastic flow on the grain boundaries depending on the concentration was studied. We apply a similar approach which combines the grain growth with the segregation of a dopant on the grain boundaries, the GB diffusion and the dependency of the mobility on the segregation.

The paper is organized as follows. The experimental procedure is described in Section 2. The combined model is introduced and the model parameters are described in section 3. The results of the simulation for different cases are presented in Section 4. Then we conclude with discussion and conclusion in sections 5 and 6.

2. Experimental data

For the fabrication of Ox-CMC mini-composites, 3000 den Nextel^{TM} 610 fibers (d 10 12 m, 3 M) were initially thermally desized at 700 C for 2 h in a LHT 04/17 chamber furnace (Nabertherm GmbH, Lilienthal, Germany). The fibers contain 99% Al_2O_3, 0.7 wt% Fe_2O_3 and 0.3% SiO_2 [44]. For the preparation of the matrix, two different alumina powders (d 150 nm, Baikowski, France) without and with 480 ppm MgO dopant were used. Tube-shaped paper molds were used to fabricate the mini-composites in cylindrical shape. After the fiber infiltration, the specimens were dried and the mini-composites were sintered in the same furnace used for fiber desizing at 1200 C for 2 h. In order to investigate the performance of the MgO dopant at higher temperatures, the sintered samples were heat treated at 1200 C, 1300 C and 1400 C for 2 h. For all thermal exposures, a heating rate of 100 K/h and a cooling rate of 300 K/h were used.

For the grain size analysis, the mini-composites were embedded in epoxy for surface preparation, e.g., grinding and polishing. Afterwards, the epoxy was thermally extracted for the subsequent thermal etching to reveal the grain boundaries of the fibers and matrix. Thermal etching temperature were performed at 1100 1300 C with 30 min of dwell time for all samples. Pictures of the microstructure of fibers were taken with a scanning electron microscope (SEM) ZEISS Supra 40 (ZEISS,

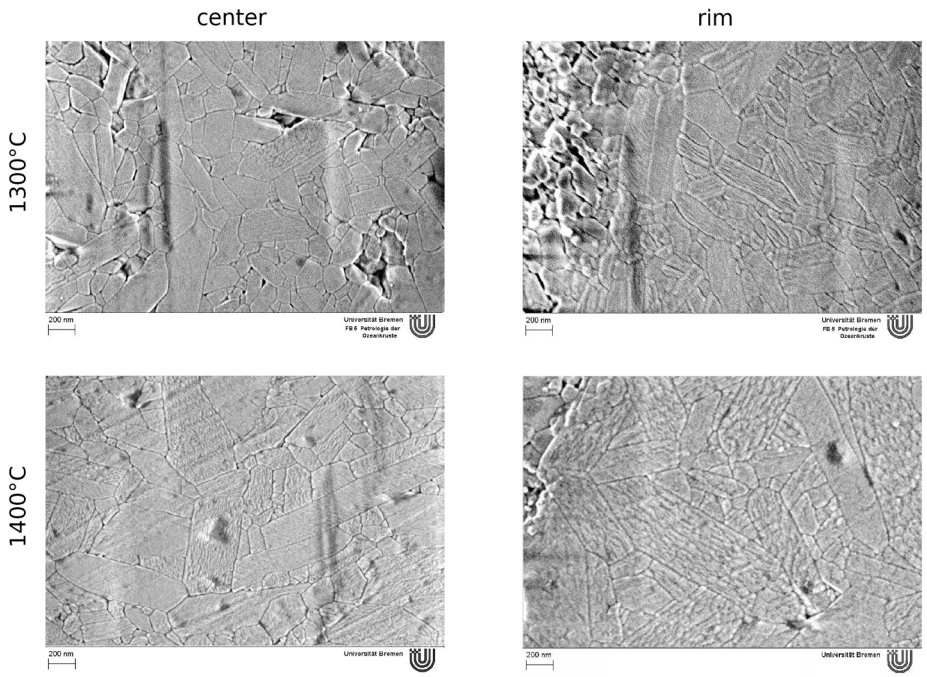

Fig. 1. SEM images of the microstructure in the fiber without dopant after the heat treatment for 2 h: (top) 1300 C; (bottom) 1400 C; (left) in the center of the fibers; (right) on the rim of the fibers.

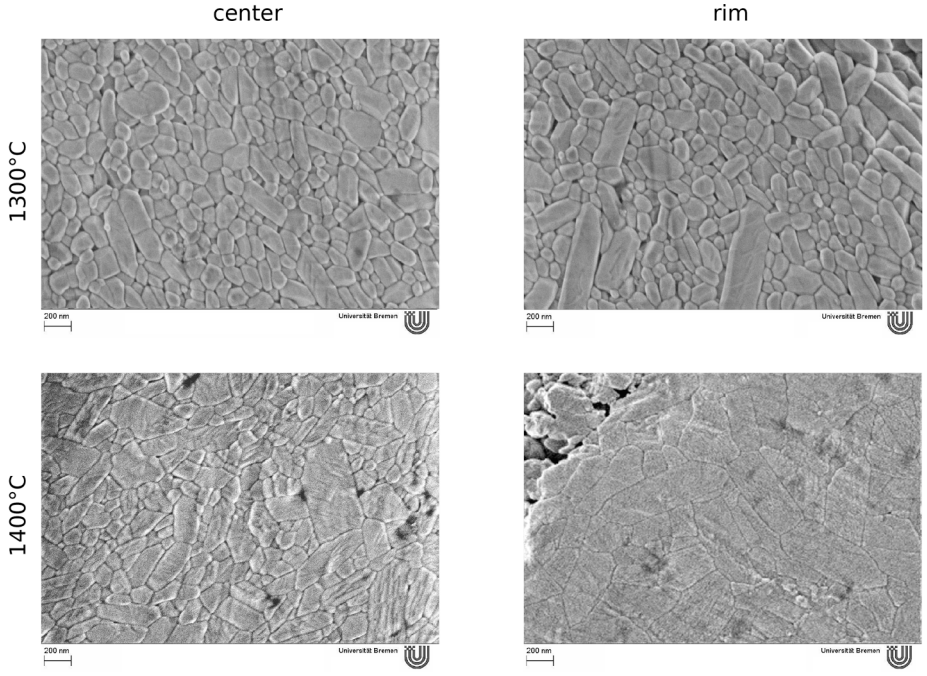

Fig. 2. SEM images of the microstructure in the fiber embedded in alumina matrix with MgO dopant after the heat treatment for 2 h: (top) 1300 C; (bottom) 1400 C; (left) in the center of the fibers; (right) on the rim of the fibers.

Oberkochen, Germany) on the center of the fibers cross-section and on the rim. Grain-size analysis was done by using the freeware *ImageJ*. The corresponding average grain size (the square root of the average area) and the standard errors are listed in Table 1. Since the grains in the fiber show an elongated shape at higher temperatures, the feret diameter was selected to represent the length of the grains. The corresponding average and maximum feret diameters in the center and on the rim of a fiber are listed in Table 1. Note that the maximum ferret can also depend on the observation window. For comparison, the same procedure was done on fibers alone, i. e., as-received condition. Examples of the microstructures of fibers after heat treatment are shown in Figs. 1 and 2. The picture size is about 2180 3056 nm^2 (see the scale bars).

3. Model description

Our purpose is to develop an effective method to simulate the grain growth in ceramic fibers embedded in a ceramic matrix with various solvent components which diffuse along the grain boundaries in the

fibers and vice versa and influence the grain size evolution during the heat exposure. For this aim, we apply the multi-phase model for the isotropic grain growth and extend it by the GB diffusion and segregation. For the simulation of the anisotropic abnormal grain growth (see cases 4 and 5 in Section 4), we will use the phase-field model developed in [40] with the anisotropic interface energy and variable interface mobility.

We assume that our physical system contains N grains which are described by N phase fields $\phi_\alpha \in [0,1]$, $\alpha = 1 \ldots N$, which are components of a vector $\boldsymbol{\phi}$. The phase fields are used to distinguish grains with different crystallographic orientations.

The total free energy functional of the system is given by

$$F = \int_V \left(f_{gb}(\boldsymbol{\phi}, \nabla\boldsymbol{\phi}) + f_{ch}(c, \boldsymbol{\phi}) \right) dV, \tag{1}$$

where f_{gb} is the free energy density of grain boundaries and f_{ch} is the chemical free energy density of the composition.

The free energy density of grain boundaries is expanded into the following terms

$$f_{gb}(\boldsymbol{\phi}, \nabla\boldsymbol{\phi}) = \sum_{\alpha,\beta,\alpha\neq\beta}^{N} \frac{4\sigma_{\alpha\beta}}{\eta} \left(-\frac{\eta^2}{\pi^2} \nabla\phi_\alpha \cdot \nabla\phi_\beta + |\phi_\alpha \phi_\beta| \right), \tag{2}$$

where η is a model interface width, $\sigma_{\alpha\beta}$ is the energy of a dual interface.

The chemical free energy density is expressed as

$$f_{ch}(\boldsymbol{c}, \boldsymbol{\phi}) = f_0 + \sum_i \frac{X_i c_i^2}{2} (1 - s_i g(\boldsymbol{\phi})), \tag{3}$$

where f_0 is the chemical energy density without dopants, c_i is the concentration of a dopant in units of mole fraction, $g(\boldsymbol{\phi}) = \sum_{\alpha,\beta,\alpha\neq\beta}^{N} \phi_\alpha \phi_\beta$ is the function responsible for the grain boundaries, X_i is a thermodynamic factor, and s_i is the segregation coefficient.

The evolution equation for the phase field variables is the Ginzburg–Landau equation for non-conserved field with Lagrange multiplier:

$$\frac{\partial \phi_\alpha}{\partial t} = -\frac{\pi^2}{8\eta} \sum_{\beta\neq\alpha}^{n} \frac{\mu_{\alpha\beta}}{n} \left(\frac{\delta F}{\delta \phi_\alpha} - \frac{\delta F}{\delta \phi_\beta} \right), \tag{4}$$

where $\mu_{\alpha\beta}$ (in units of $m^4/(Js)$) are mobilities on dual interfaces and n is the number of grains which are in local contact.

Inserting the free energy we get the evolution equation explicitly

$$\frac{\partial \phi_\alpha}{\partial t} = \sum_{\beta\neq\alpha}^{n} \frac{\mu}{n} \left\{ \sigma \left[\nabla^2\phi_\alpha - \nabla^2\phi_\beta + \frac{\pi^2}{\eta^2}(\phi_\alpha - \phi_\beta) \right] + \frac{\pi^2}{8\eta} \frac{\sum_i X_i c_i^2 s_i}{2} (\phi_\alpha - \phi_\beta) \right\}. \tag{5}$$

Here we assume the same mobility for all grains $\mu_{\alpha\beta} = \mu$ and the same surface energy $\sigma_{\alpha\beta} = \sigma$.

The evolution equations for the concentration have the form of the diffusion equation in the dilute solution limit

$$\frac{\partial c_i}{\partial t} = \nabla \cdot \left[\frac{D_i^{eff}}{X_i} \nabla \frac{\delta F}{\delta c_i} \right] \tag{6}$$

with the effective diffusion coefficient defined as

$$D_i^{eff} = D_i^{gb} \sum_{\alpha,\beta,\alpha\neq\beta}^{N} \phi_\alpha \phi_\beta + D_i^{L} \sum_{\alpha}^{N} \phi_\alpha^2 (3 - 2\phi_\alpha), \tag{7}$$

where D_i^{gb} is the GB diffusion coefficients, and D_i^{L} is the lattice diffusion. The model function $h(\phi_\alpha) = \phi_\alpha^2(3 - 2\phi_\alpha)$ guarantees non-zero values of diffusivity in grains and zero values outside grains. The function becomes significant if the system contains pores or different phases. It is assumed $D_i^{gb} \gg D_i^{L}$. The diagonal component of diffusion matrix are set to zero. The real GB diffusion coefficients should be recalculated using the ratio between the real grain boundary width, δ, and the interface width

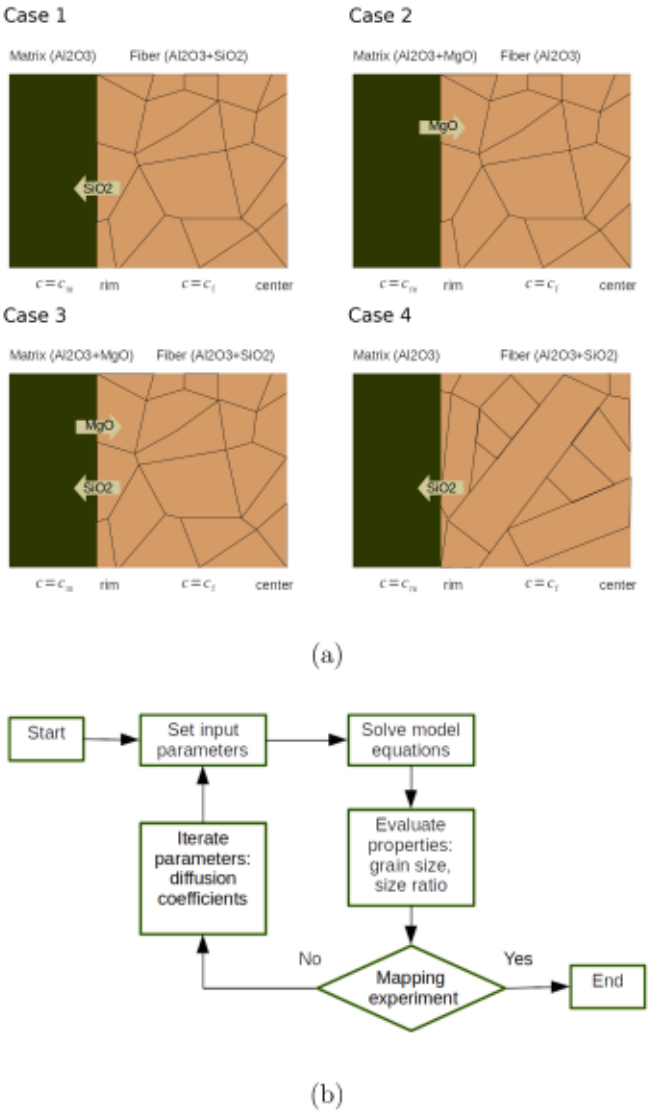

Fig. 3. (a) Scheme of simulation cases; (b) scheme of the inverse method.

in the phase-filed model which is equal to $\int_{-\eta/2}^{\eta/2} \phi(1-\phi)dx = \frac{\eta}{8}$. From the constraint that the real total flux over the grain boundary equals the total flux over the grain boundary in the phase-field model, we obtain $D_i^{gb}(\text{real}) = D_i^{gb}(\text{model})\frac{\eta}{8\delta}$. Note that the real concentration of dopants on the grain boundary should by larger than the simulated value also by factor $f = \frac{\eta}{8\delta}$.

Inserting the free energy in (6) and applying $\nabla \frac{\delta F}{\delta c_i} = \frac{\partial^2 F}{\partial c_i^2} \nabla c_i$, where $\frac{\partial^2 F}{\partial c_i^2} = X_i$ is the thermodynamic factor, we get the evolution equation in the form

$$\frac{\partial c_i}{\partial t} = \nabla \cdot \left[D_i^{eff} (1 - s_i g(\phi)) \nabla c_i \right] - \nabla \cdot \left[s_i c_i D_i^{eff} \nabla g(\phi) \right]. \tag{8}$$

In the dilute solution limit the equation is valid for both components MgO and SiO_2.

The dependency of the boundary mobility on the concentration is defined by

$$\mu(c) = \mu_0 (1 + c(t)/c_m)^{-2}, \tag{9}$$

where c_m is a phenomenological parameter which indicates the concentration on the grain boundary which reduces the mobility by four times. In case of two components, the concentration dependency be-

Table 2
Model parameters used in the simulations.

Parameter	Symbol	Value	Units
Grid spacing	x	5 10 ^{9}	m
Interface width		5.4 x	m
Time step	t	varying	s
Interface energy		1.5	J/m^2
Lattice diffusion coefficient	D	0 01D	m^2/s
GB diffusion coefficient	D	varying	m^2/s
Initial concentration	c_0, MgO	0 3	%
	c_0, SiO$_2$	0 05	
GB concentration	c_m, MgO	0 066	%
	c_m, SiO$_2$	0 4	
Segregation coefficient	s	2	
Case 1 (SiO$_2$)			
Interface mobility	$_0$, 1300 C	4 4 10 ^{18}	m^4/(Js) [20]
	$_0$, 1400 C	1 8 10 ^{17}	
GB diffusion coefficient	D1	5 6 10 ^{16}	m^2/s
	D2	1 2 10 ^{15}	
	D3	2 9 10 ^{16}	
	D4	5 6 10 ^{16}	
Case 2 (MgO)			
Interface mobility	$_0$, 1200 C	5 5 10 ^{19}	m^4/(Js)
	$_0$, 1400 C	4 4 10 ^{18}	
GB diffusion coefficient	D5	3 6 10 ^{16}	m^2/s
	D6	7 2 10 ^{16}	
	D7	2 9 10 ^{15}	
	D8	5 8 10 ^{15}	
Case 3 (SiO$_2$ and MgO)			
Interface mobility	$_0$, 1300 C	4 4 10 ^{18}	m^4/(Js)
	$_0$, 1400 C	1 8 10 ^{17}	
GB diffusion coefficient	D9 Si	1 1 10 ^{16}	m^2/s
	D10 Si	2 9 10 ^{16}	
	D11 Mg	6 8 10 ^{16}	
	D12 Mg	5 2 10 ^{15}	
Case 4 (SiO$_2$, abnormal)			
Interface mobility	$_0$, 1400 C	1 8 10 ^{17}	m^4/(Js)
GB diffusion coefficient	D13	2 9 10 ^{16}	m^2/s
	D14	5 8 10 ^{16}	

comes

(10)

where c_m^i are the corresponding phenomenological parameters of components.

4. Simulation procedure and results

4.1. Simulation procedure and model parameters

We consider the following cases: 1) SiO$_2$ diffuses from the fiber into the matrix; 2) MgO diffuse from the matrix into the fiber; 3) combined diffusion of SiO$_2$ and MgO; 4) abnormal growth in presence of the SiO$_2$ diffusion. The general scheme of simulation tests is given in Fig. 3. Cases 1 and 3 represent the composite without dopant and with MgO dopant in the matrix, respectively. Without dopant means the presence of SiO$_2$ as a standard additive in Nextel fibers. Case 2 is necessary to roughly estimate the value of the GB diffusion coefficient of MgO. Case 4 attends to show the influence of the abnormal and anisotropic grain growth on the grain size distribution on example of SiO$_2$ diffusion from the fiber into the matrix. The real diffusion of silica and magnesia occurs by the diffusion of oxygen, Si and Mg ions. For the sake of simplicity, we will assess in the following the diffusion coefficients of Mg and Si ions and omit the diffusion of oxygen ions.

The diffusion is modeled in the 2D box of size 436 612 x^2 (2118 3060 nm^2) filled by 720 grains in cases 1 and 2 and in the 2D box of size 436 1049 x^2 (2118 5248 nm^2) filled by 1192 grains in cases 3 and 4. The size in x-direction is circa 50% of the fiber diameter. The boundary conditions for phase-field parameters are periodic on the top and bottom of the box, and no flux on the left and right sides of the box. The boundary conditions for concentrations are periodic on the top and bottom of the box, no flux on one right side, and a constant concentration on the left side where the rim of the fiber is joined with the matrix. The model Eqs. (5) and (8) are solved by finite difference method with the forward Euler method. The time step was adjusted accordingly using the numerical stability criterion for diffusion 2D t x^2 1 and for grain growth 2 t x^2 1.

The model parameters are listed in Table 2. The GB mobility in pure alumina without dopant is taken from experiments [20]. The interface energy is chosen according to the first-principal calculations presented in Refs. [45,46]. The GB diffusion coefficient varies for different cases. The segregation coefficient is chosen as s 2. It means that according to Eq. (3), the part of the chemical energy responsible for dopants decreases on a grain boundary, where 0 5, in two times. The value is chosen in accordance to the theoretical predictions of the energy of ion segregation to an alumina grain boundary [8].

The values of GB diffusion coefficients were determined from the tests by the inverse method which is described in the next section. The diffusion coefficients D1 D14 in Table 2 are used as examples.

4.2. Inverse method

The inverse method is used with the aim to simulate the diffusion of dopants between fiber and matrix in order to make predictions about the chemical composition of matrix to fully or partially inhibit the grain growth. However, we do not have the proper diffusion coefficient for each element in alumina, nor how two elements can influence the diffusion of each other. Due to slower diffusion of silica and magnesia, the local amount of dopant components cannot be measured. We do however, know that these elements change the grain growth kinetics of the fibers, resulting in different grain sizes after the exposures. Therefore, we try to change the GB diffusion coefficients to achieve a similar microstructure.

The method is used to adjust the unknown GB diffusion coefficients until the microstructure parameters match the measured experimental values. The microstructure parameters used for mapping the experiment are the average grain size in the center of fiber, d_{center}, and the ratio between the sizes on the rim and in the center d_{rim} d_{center}. The algorithm of the inverse method is sketched in Fig. 3(b). The iterations are repeated until the deviation between the modeling and experiment results becomes smaller than the standard error in the experiment.

In case 1, we start with the experimental interface mobility $_0$ without dopant and adjust the GB diffusion coefficient of Si. In case 2, we use the mean interface mobility from case 1, which is reduced due to presence of silica, and analyse the effect of the GB diffusion coefficient of Mg on the grain growth. In case 3, we use the experimental interface mobility $_0$ and the GB diffusion coefficient of Si defined in case 1, and adjust the GB diffusion coefficient of Mg. During the inverse simulation tests, bisection method is used for the optimization of one parameter, i.e. diffusion coefficient, while the other parameters are fixed.

4.3. Case 1

The diffusion of Si from the fiber into the matrix is modeled at two temperatures 1300 C and 1400 C. The GB diffusion coefficients were varying in the region from 2 10 ^{17} to 2 10 ^{15} m^2/s during the

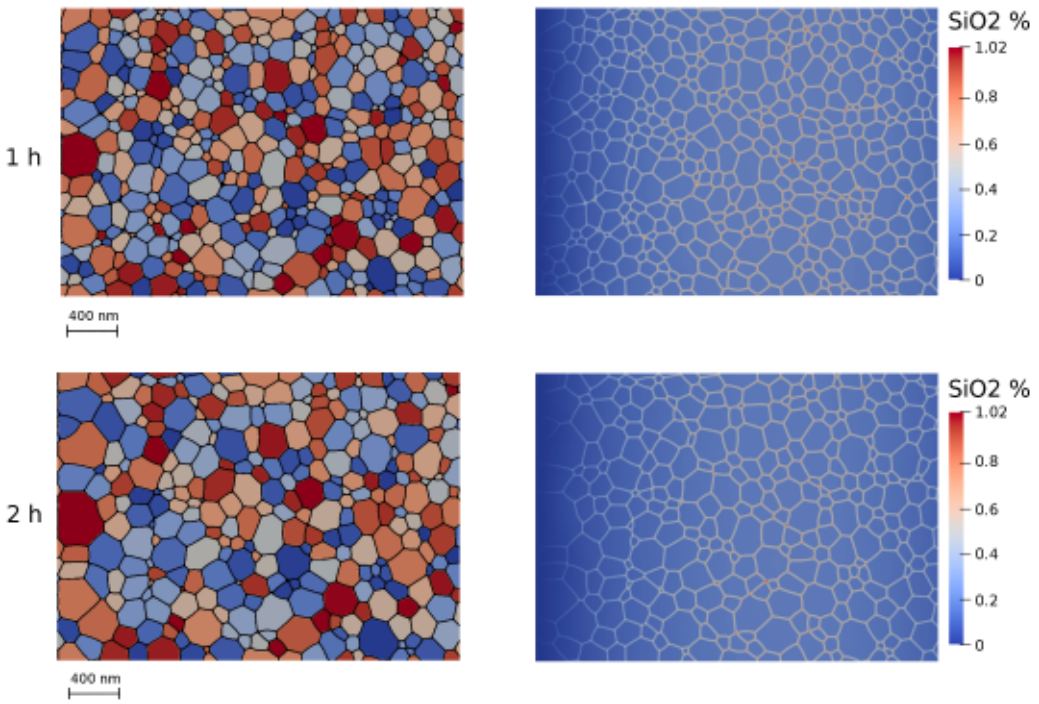

Fig. 4. Simulation results in case 1 after heat treatment during 1 h (top) and 2 h (bottom) at 1300 °C with $D1(Si)$: (left) grain microstructure in the fiber embedded in alumina matrix; (right) concentration field for SiO_2. The matrix/fiber boundary is on the left site.

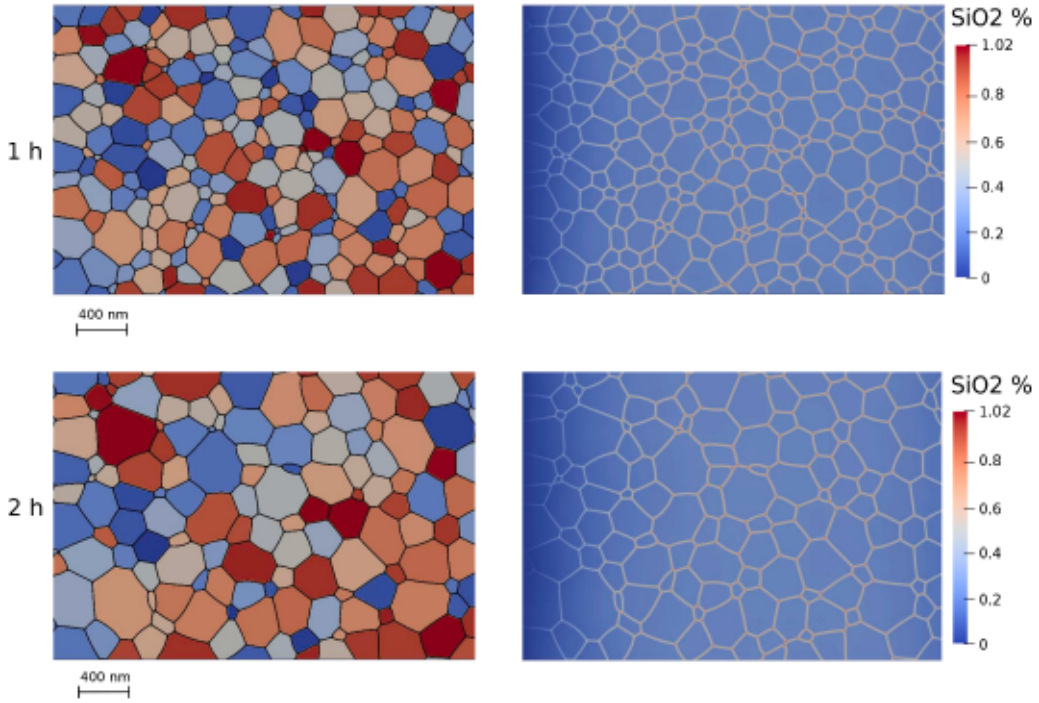

Fig. 5. Simulation results in case 1 after heat treatment during 1 h (top) and 2 h (bottom) at 1400 °C with $D3(Si)$: (left) grain microstructure in the fiber embedded in alumina matrix; (right) concentration field for SiO_2. The matrix/fiber boundary is on the left site.

inverse method to fit the experimental properties. The example coefficients are listed in Table 2. The initial concentration of SiO_2 in the fiber is set to $c_0 = 0.3\%$. The concentration on the right side of the box is set to zero, which mimics the concentration in the matrix.

The simulated microstructure and the concentration distribution are shown in Figs. 4 and 5 for 1 and 2 h at 1300 °C and 1400 °C, respectively.

The time evolution of the average grain size for two temperatures and different diffusion coefficients is shown in Fig. 6(a). The comparison to the theoretical curve, $d^2 = d_0^2 + \mu\sigma t$, where μ is calculated by Eq. (9) using the mean concentration on the grain boundary, shows that the grain growth rate increases if Si diffuses from the fiber along the grain boundaries. The increase of the diffusion coefficient from $D1$ to $D2$ and from $D3$ to $D4$ affects the growth kinetics and this effect is larger at the higher temperature.

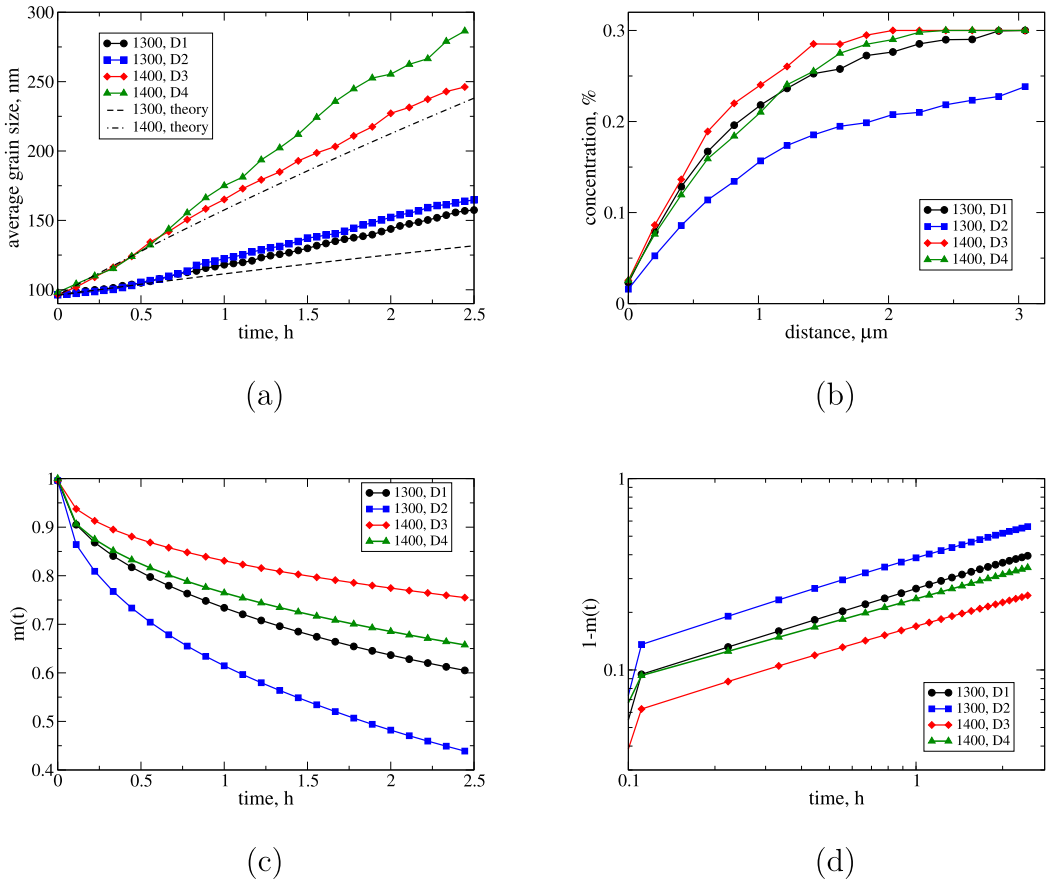

Fig. 6. Simulation results in case 1 at 1300 C and 1400 C with different GB diffusion coefficients: (a) grain size evolution in the fiber with Si diffusion from the matrix to the fiber during heat treatment, straight red lines are the theoretical dependencies without diffusion from the sample; (b) concentration distribution of SiO_2 in the fiber after heat treatment during 2 h, the distance from the matrix/fiber boundary is plotted on the x-axis; (c) time evolution of the SiO_2 average concentration in the fiber, $m\ t$; (d) logarithmic plot of 1 $m\ t$.

The concentration distribution in the sample for different diffusion coefficients after 2 h of the heat treatment is shown in Fig. 6(b) for 1300 C and 1400 C. The matrix is on the left side and the diffusion flow is directed from the right to the left. The average concentration in sections decreases with increasing diffusion coefficient.

The fitting of the concentration distribution at 2 h by the error function gives:

— (11)

where the fitting parameters are the following:

Parameter	1300 C, $D1$	1300 C, $D2$	1400 C, $D3$	1400 C, $D4$
x_0	1.3382	1.8038	1.1193	1.5189
c_0	0.033	0.031	0.029	0.033
c_1	0.2572	0.2258	0.2707	0.2722

The comparison to the homogeneous solution of the diffusion equation in two semi-infinite bodies gives x_0 $4D$ t 8, where factor 8 comes from the interface width in the phase-filed model.

Fig. 6(c) and (d) show the evolution of a total mass in the fiber for different GB diffusion coefficients and temperatures. The kinetic of this diffusion process can be also analysed by means of the calculation of a total mass, $m\ t$ $c\ t$ c_0, where $c\ t$ is the volume averaged concentration in the sample and c_0 is the dopant concentrations at the end of the equilibration process (i.e the concentration of silica in the fibers). $m\ t$ is a reduced mass exchanged between the fiber and a constant diffusion source. The analytical model which describe the process of GB diffusion was proposed by Preis et al. [36] for spherical and square grains. According to this model, in the case of a constant grain structure and the fast GB diffusion, the total mass recalculated in the semi-logarithmic plot is a linear relaxation curve with an effective coefficient of proportionality D . Fig. 6(c) shows the evolution of the total mass in the fiber for different GB diffusion coefficients and temperatures. As it can be seen in Fig. 6(d), the relaxation curves tend to a logarithmic dependency. The best fit of the time dependencies is a phenomenological equation with power law:

(12)

where a and n are the fitting parameters, t is given in hours. The correlation coefficient is 0.99987. The fitting parameters are the following:

Parameter	1300 C, $D1$	1300 C, $D2$	1400 C, $D3$	1400 C, $D4$
a D	0.2651	0.3820	0.1681	0.2353
a	1 11 10^7	1 10 10^7	9 84 10^6	9 84 10^6
n	0.4550	0.4416	0.4285	0.4201

It can be seen that a and n depend on the temperature and do not depend on the diffusion coefficient. The temperature dependency is obviously due to the interface mobility and hence due to the different average grain size.

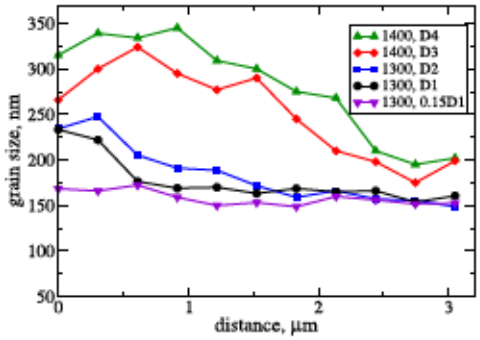

Fig. 7. Grain size distribution in case 1 in the fiber with SiO_2 diffusion after heat treatment during 2 h at 1300 °C and 1400 °C for different GB diffusion coefficients. The distance from the matrix/fiber boundary is plotted on the x-axis.

Table 3
Comparison of experimental and modeling results: ratio between the rim and the center and the average size in the center of the fiber. The data for the feret diameter are shown in brackets.

Conditions		Experiment		Modeling		
		d_{rim}/d_{center}	d_{center}, nm	d_{rim}/d_{center}	d_{center}, nm	Case, D^{gb}
1300 °C	no dopant	1.1(1.18)	161 (233)	1.15	155	1, 0.15D1
	with MgO	1.1(1.10)	124 (168)	1.05	128	3, D9 & D11
1400 °C	no dopant	1.32(2.3)	225 (336)	1.50	212	1, D3
	no dopant	1.32(2.3)	225 (336)	1.48(1.8)	245 (360)	4, D13
	with MgO	1.50 (1.95)	153 (338)	1.25	175	3, D10 & D12

The grain size distribution profile in Fig. 7 after 2 h of the heat treatment was calculated by using the sections in the direction normal to the diffusion flow similar to the concentration distribution profile. At low temperature (1300 °C), the difference in grain size on the rim and in the center is about $d_{rim}/d_{center} = 1.39$ for the diffusion coefficients $D1$ and $D2$. That is much more than in the experimental results in Table 1. The diffusion coefficient $0.15D1 = 8.4 \times 10^{-17}$ m^2/s at 1300 °C gives the best fit with the experiment with $d_{rim}/d_{center} = 1.15$. At high temperature (1400 °C), the difference is also significant and the ratio of grain sizes reaches $d_{rim}/d_{center} = 1.5$. Comparing to the experimental results in Table 1 shows the best fit at 1400 °C for the diffusion coefficient $D3 = 2.9 \times 10^{-16}$ m^2/s. The comparison of the experimental and modeling ratio of grain sizes between the rim and the center is shown in Table 3. The modeling ratio in case 1 is a little larger than in the experiment.

4.4. Case 2

The diffusion of Mg from the matrix into the fiber is modeled for two temperatures, 1200 °C and 1400 °C, with the concentration $c_0 = 0.05\%$ (500 ppm) in the matrix and 0% in the fiber. The lower temperature is changed now compared to cases 1 and 3 due to the much faster diffusion in this case. The effect of Mg diffusion can be observed in the experiment already at 1200 °C, whereas the effect of silica at this temperature is not evident. The applied GB diffusion coefficients and the interface mobility are listed in Table 2. No diffusion of silica from the fiber to the matrix is simulated. To mimic the presence of silica in the fiber, the interface mobility is chosen to be four times smaller than in case 1. The concentration of MgO on the left boundary of the box is set to c_0.

The simulated microstructure and the concentration profile of MgO after 1 and 2 h of the heat treatment are shown in Figs. 8 and 9 at 1200 °C and 1400 °C, respectively. The matrix is on the left boundary of the simulation box and the diffusion flow of Mg is directed from the left to the right.

The average grain size evolution is shown in Fig. 10(a) for two temperatures and different diffusion coefficients. The comparison to the theoretical curve, $d^2 = d_0^2 + \mu_0 \sigma t$, for 1200 °C shows that the grain

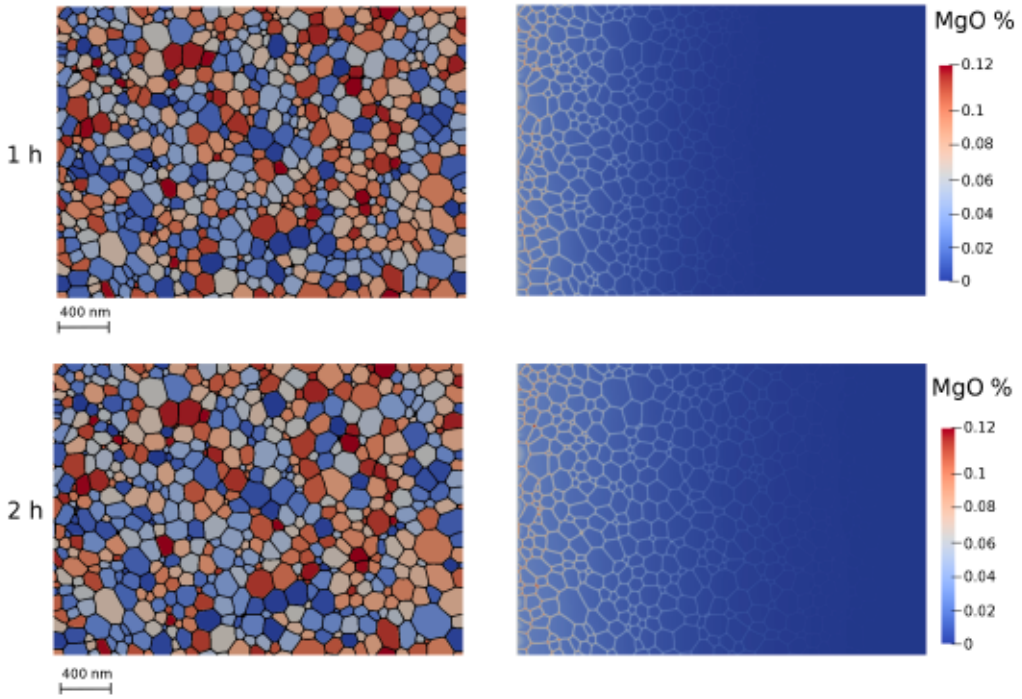

Fig. 8. Simulation results in case 2 after heat treatment during 1 h (top) and 2 h (bottom) at 1200 °C with $D6$(Mg): (left) grain microstructure in the fiber embedded in alumina matrix; (right) concentration field for MgO. The matrix/fiber boundary is on the left site.

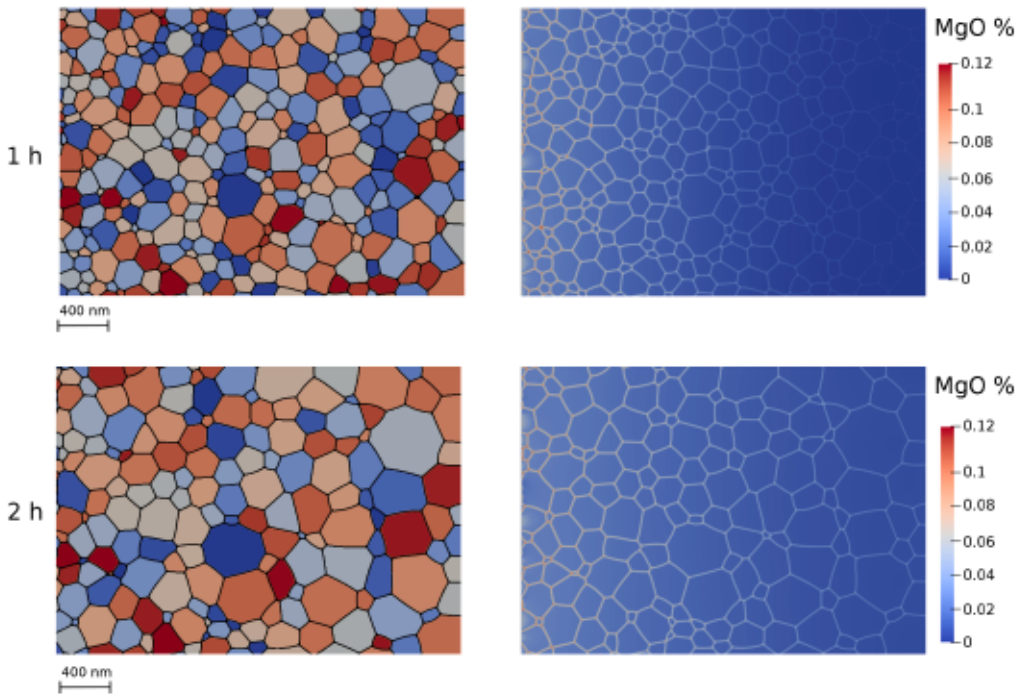

Fig. 9. Simulation results in case 2 after heat treatment during 1 h (top) and 2 h (bottom) at 1400 °C with *D7*(Mg): (left) grain microstructure in the fiber embedded in alumina matrix; (right) concentration field for MgO. The matrix/fiber boundary is on the left site.

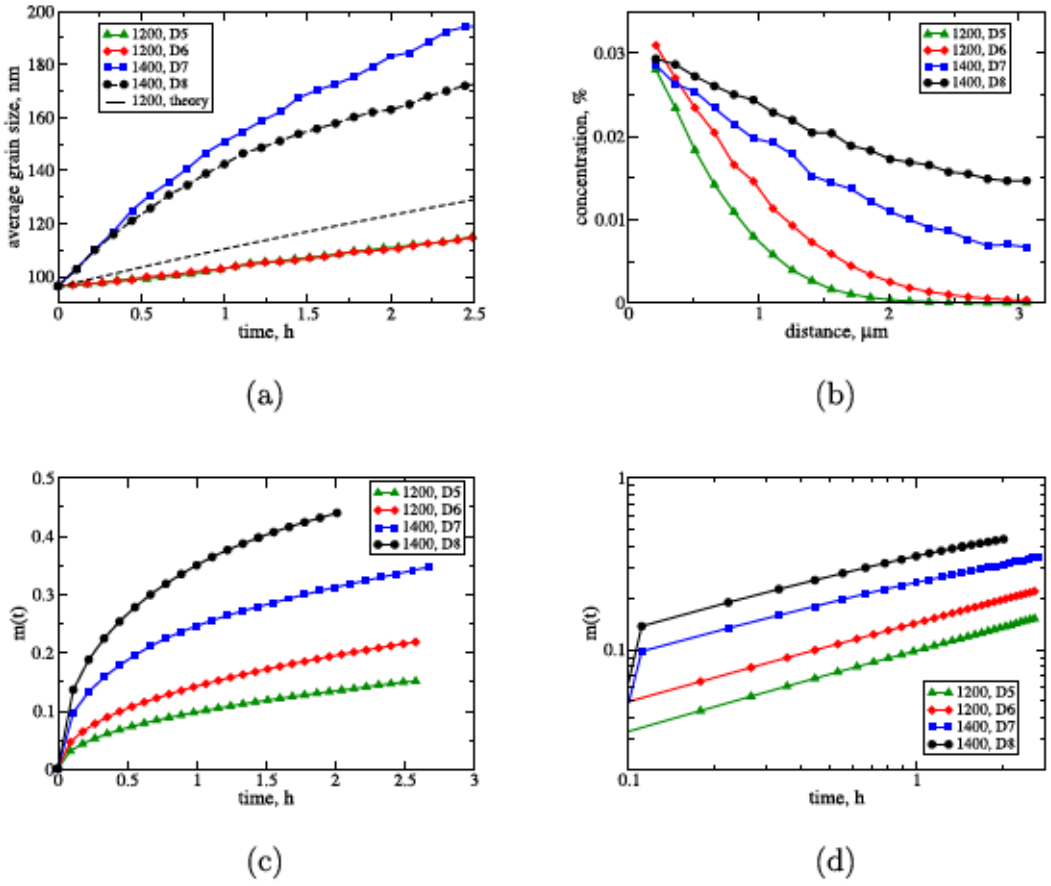

Fig. 10. Simulation results in case 2 at 1200 °C and 1400 °C with different GB diffusion coefficients: (a) grain size evolution in the fiber with MgO diffusion from the matrix to the fiber during heat treatment; (b) concentration distribution of MgO in the fiber after heat treatment during 2 h, the distance from the matrix/fiber boundary is plotted on the *x*-axis; (c) time evolution of the MgO average concentration in the fiber, $m(t)$; (d) logarithmic plot of $m(t)$.

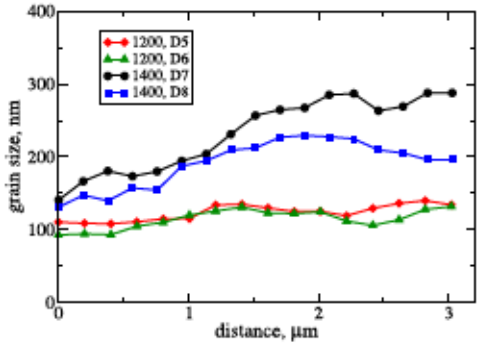

Fig. 11. Grain size distribution in case 2 in the fiber with Mg diffusion after heat treatment during 2 h at 1200 °C and 1400 °C for different GB diffusion coefficients. The distance from the matrix/fiber boundary is plotted on the x-axis.

growth rate decreases at least in two times if Mg diffuses in the fiber along the grain boundaries. The increase of the GB diffusion coefficient does not effect the growth rate at 1200 °C. However, at the higher temperature (1400 °C) the effect on the growth kinetics is significant.

The average concentration distribution in the sample for the different diffusion coefficients after 2 h of the heat treatment is shown in Fig. 10(b). The calculation was carried out by using the sections in the direction normal to the diffusion flow. The matrix is on the left side and the diffusion flow is directed from the left to the right so that the distance is measured from the rim to the center. The average concentration in sections increases with increasing diffusion coefficient. At higher temperature MgO fills the grain boundaries of the fiber until the center and, therefore, it should decrease the grain growth rate here.

The fitting of the concentration distribution by the error function gives:

$$\bar{c} = c_0\left(1 - \mathrm{erf}\left(\frac{x}{x_0}\right)\right), \tag{13}$$

where the fitting parameters a and b are the following:

Parameter	1200 °C, D5	1200 °C, D6	1400 °C, D7	1400 °C, D8
x_0	1.18	1.57	3.22	5.55
c_0	0.0355	0.0360	0.0301	0.0299

Here x_0 is proportional to $\sqrt{D^{gb}}$ with the precision ±12%.

Fig. 10(c) and (d) describe the time evolution of the concentration field for different GB diffusion coefficients and temperatures. For the calculation of the total mass, $m(t) = \bar{c}(t)/c_0$, the dopant concentrations at the beginning of the equilibration process (i.e. the initial concentration of MgO in the matrix) was used. The relaxation curves are presented in Fig. 10(d) as logarithmic plots of $m(t)$ versus time. They can be fitted by a phenomenological equation

$$m(t) = a\sqrt{D^{gb}}t^n, \tag{14}$$

where t is the time in hours, a and n are the fitting parameters:

Parameter	1200 °C, D5	1200 °C, D6	1400 °C, D7	1400 °C, D8
$a\sqrt{D^{gb}}$	0.0983	0.1428	0.2423	0.34445
a	5.2×10^6	5.3×10^6	4.5×10^6	4.5×10^6
n	0.4587	0.4518	0.3720	0.3791

The correlation coefficient is 0.99987. It can be seen that these parameters change with the temperature. This is due to change of the average grain size and the length of the grain boundaries.

The grain size distribution profile is plotted in Fig. 11 after 2 h. It can be seen that at low temperature the difference in grain size on the rim and in the center of the fiber is small. However, at high temperature (1400 °C) the difference is significant, the ratio between grain sizes is about $d_{rim}/d_{center} = 0.8$.

4.5. Case 3

The combined diffusion of Si from the fiber into the matrix and Mg

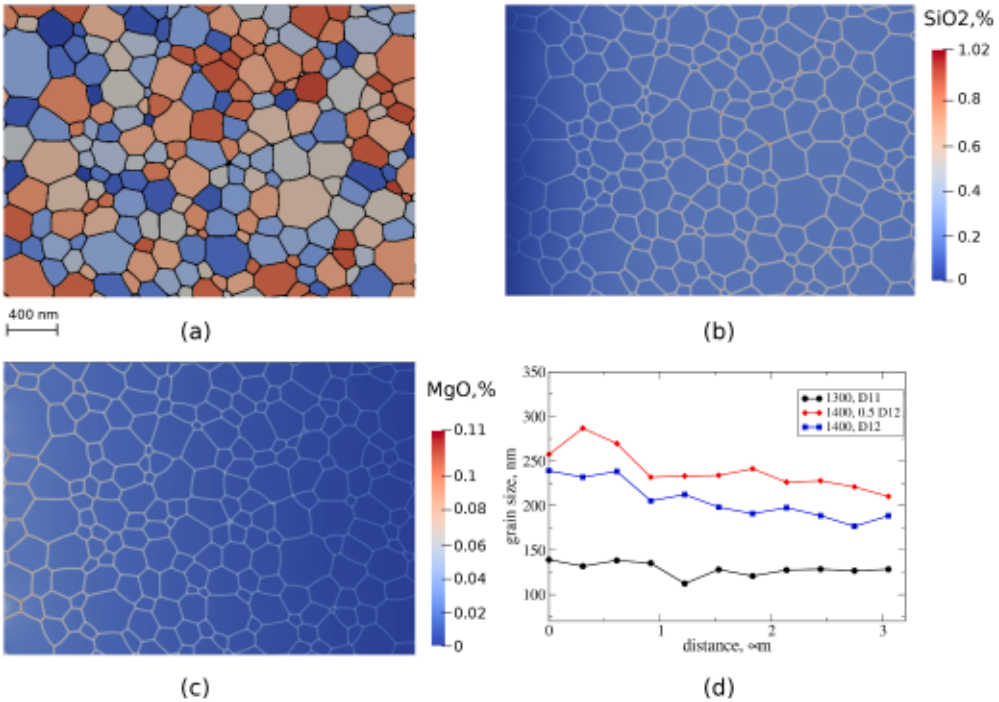

Fig. 12. Simulation results in case 3 after heat treatment during 2 h at 1400 °C with $D10$(Si) and $D12$(Mg): (a) Simulated grain microstructure in the fiber embedded in alumina matrix; (b) concentration filed for SiO_2; (c) concentration field for MgO; (d) grain size distribution in the fiber. The matrix/fiber boundary is on the left site.

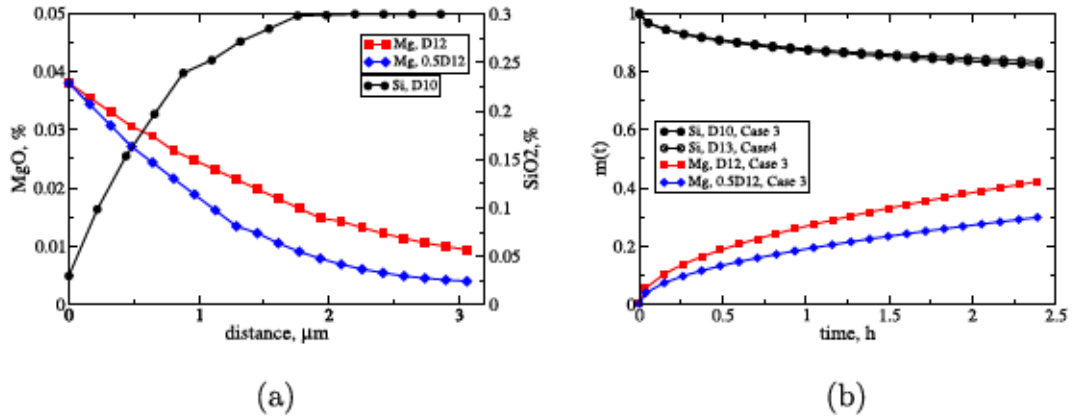

Fig. 13. Simulation results in case 3 at 1400 °C: (a) concentration distribution of MgO and SiO_2 in the fiber after heat treatment during 2 h; (b) time evolution of the MgO and SiO_2 average concentration in the fiber for different GB diffusion coefficients, comparison to case 4.

Table 4
Comparison of the real GB diffusion coefficients defined in this work with the lattice diffusion coefficients. The diffusion coefficients are given in units m^2/s.

T	Element	D^{gb} (model)	D^{gb} (real)	D^{L} [Ref]	$D^{gb}(real)/D^{L}$
1300 °C	Si	8.4×10^{-17}	1.4×10^{-15}	1.7×10^{-19} extr. [10]	8.3×10^{3}
	Mg	6.8×10^{-16}	1.2×10^{-14}	2.2×10^{-18} extr. [10]	5.4×10^{3}
	Al	–	–	4.0×10^{-19} [10]	3.5×10^{3} [48]
1400 °C	Si	2.9×10^{-16}	4.9×10^{-15}	1.5×10^{-18} extr. [10]	3.5×10^{3}
	Mg	5.2×10^{-15}	8.8×10^{-14}	1.9×10^{-17} extr. [10]	4.4×10^{3}
	Al	–	–	3.5×10^{-18} [10]	-

into the fiber is simulated at the temperatures 1300 °C and 1400 °C. From the experimental data in Table 1, we can see that the grain size decreases in the center and on the rim of the fiber in presence of MgO dopant whereas the Si diffusion affects only the rim causing here the larger grain size. Hence we can assume that the Mg diffusion is much faster than Si diffusion and Mg have time to fill the fiber till the center. The diffusion coefficients listed in Table 2 are the best fit of the experimental grain size. The microstructure after 2 h of the heat treatment and the concentration field of SiO_2 and MgO is shown in Fig. 12(a)–(c). The grain size distribution profile is plotted in Fig. 12(d) for two different diffusion coefficients of Mg. The ratio of grain sizes is $d_{rim}/d_{center} = 1.25$ for both diffusion coefficients. The comparison of experimental and modeling ratio of grain sizes on the rim and in the center and the average size in the center is shown in Table 3.

The concentration distribution and the time evolution of the average concentration of SiO_2 and MgO in the fiber is shown in Fig. 13. The simulation results allow to assess the GB diffusion coefficient of Mg by the inverse method. The fitting parameters for 1300 °C are: $D9(Si) = 8.4\times10^{-17}$ m^2/s; $D11(Mg) = 6.8\times10^{-16}$ m^2/s. The fitting parameters for 1400 °C are: $D10(Si) = 2.9\times10^{-16}$ m^2/s; $D12(Mg) = 5.2\times10^{-15}$ m^2/s. The values are listed in Table 4. In summary, the diffusion coefficient of Mg is higher than that of Si in 6–7 times to fit the experimental data.

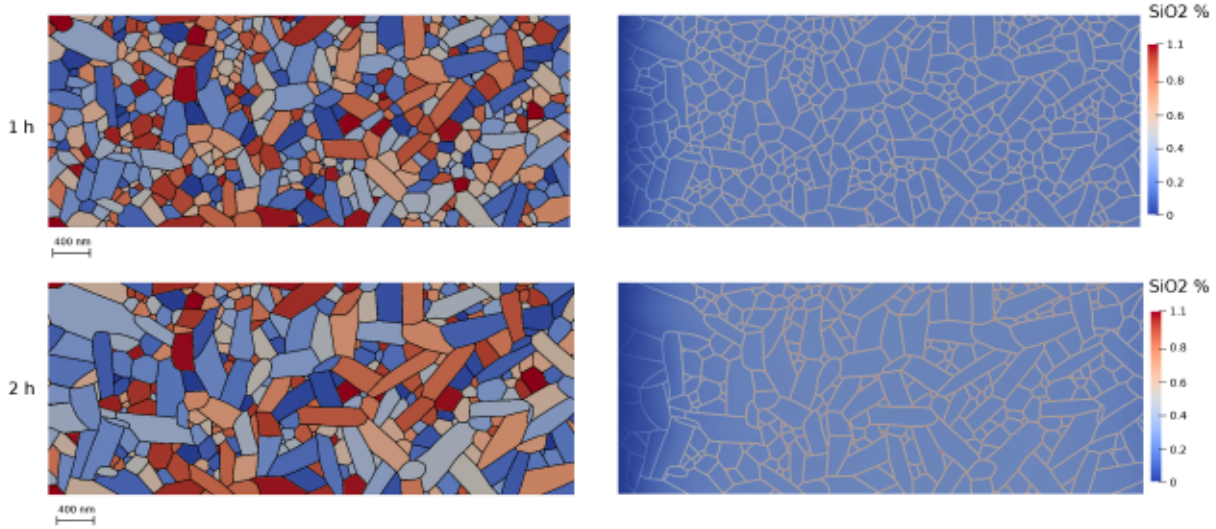

Fig. 14. Simulation results in case 4 after heat treatment during 1 h (top) and 2 h (bottom) at 1400 °C with $D13(Si)$: (left) anisotropic grain microstructure in the fiber embedded in alumina matrix; (right) concentration field for SiO_2. The anisotropic surface energy and misorientation dependent grain boundary mobility are used for the simulation of the abnormal grain growth. The matrix/fiber boundary is on the left site.

4.6. Case 4

The diffusion of Si from the fiber into the matrix is modeled at 1400 C for the abnormal grain growth. We assume in the sample the presence of 20% of abnormal grains which have a large misorientation with normal grains and hence the mobility of grain boundaries of such grains is chosen to be in 5 times higher than the mobility of grain boundary between normal grains The later assumed to be 0 45 $_0$. The values of the anisotropic surface energy and anisotropy parameter are taken from Ref. [40]. Other parameters are listed in Table 2.

The simulated microstructure in the fiber and the composition field for SiO_2 after 1 and 2 h of heat treatment is shown in Fig. 14. The estimation of the average grain size in the center and on the rim gives d 245 and d 361 nm, the ratio of grain sizes is d d 1 48 as shown in Table 4 (with GB diffusion coefficient D13).

It can be also seen in Fig. 13(b) (compare Si diffusion in case 3 and case 4) and Fig. 14 (right) (compare concentration distribution with Fig. 12(b)) that the concentration in the case of the abnormal grain growth with the Si diffusion do not show an evident difference with the results for the normal grain growth in case 3. A future work is needed to make the precise verification of the abnormal grain growth effect by means of 3D simulations.

5. Discussion

It is important to point out that the accuracy of the assessment of diffusion coefficients is determined by the statistical data of the experiment and the assumption that the grain growth kinetic can be reproduced by the isotropic model neglecting the anisotropic character of the microstructure. Nevertheless, the differences found by the modeling between diffusion coefficient of Si and Mg are significant which is confirmed by the literature data regarding the size and the charge of the cations. It is assumed in the modeling that the presence of SiO_2 in the fiber does not affect the diffusion of magnesia from the matrix and the duffusion of magnesia does not affect the diffusion of silica. However, the presence of both components on the grain boundary can affect the GB mobility.

To calculate the real diffusion coefficients, the coefficients in the model should be multiplied by factor f 8 . For the grain width in ceramic 0 2 nm, the factor is equal to 17. The comparison of the estimated real GB diffusion coefficients, D^{gb} (real) 17D^{gb} (model), with the data from the literature is given in Table 4. The lattice diffusion coefficients of Al in alumina from the literature [10] were extrapolated to Mg and Si by using the factors defined by the molecular dynamics (MD) simulation in Ref. [47]. It can be seen that the diffusion coefficient of Mg is much higher than that of Al and Si. This is also in accordance to the fact that diffusion of the cations with lower valence, e.g. Mg, is much faster than with high valence, e.q. Si [10].

Using the real GB diffusion coefficients estimated by the inverse modeling, we can find the parameters of the Arrhenius law. The activation energy of the diffusion for Mg is 435 7 kJ/mol and the prefactor is 3 5 m^2/s. The activation energy of the diffusion for Si is 273 9 J/mol and the prefactor is 1 8 10 ^{6} m^2/s. Then we can calculate the unknown diffusion coefficients at 1200 C as D^{gb}(real, Mg) 1 2 10 ^{15} m^2/s and D^{gb}(real, Si) 3 4 10 ^{16} m^2/s.

The modeling results such as the phenomenological eqs. (12) and (14) allow us to estimate the time to reach a stable concentration distribution of the dopant in the fiber. E.q. for Mg, we can find that to reach the maximum value of the concentration in the full fiber at 1400 C, m t 0 03% in Fig. 10(b), one needs 17.6 h.

The developed model with estimated parameters allows us to make the predictions of grain size distribution in the fiber (see Fig. 12(d)) by varying the dopant concentration in the matrix at different heat treatment temperatures for different dwell time.

6. Conclusion

We developed an extended model for describing GB diffusion and segregation in ceramic materials. The model is based on the multi-phase-field model of grain growth which takes into account the dependency of the GB mobility on the concentration (segregation dependency). Our considerations are restricted to the cases of silica diffusion from the fiber to the matrix and magnesia diffusion from the matrix to the fiber. The grain size distribution in the fiber after heat treatment is affected by the diffusion of dopants that leads to the different grain size on the rim of the fiber and in the center. The inverse method is applied to adjust the unknown grain boundary diffusion coefficients of dopants by comparison to the experimental grain size distribution. The analysis of the concentration distribution in the fibers shows that the simulation results are in agreement with the theoretical prediction of diffusion profiles for semi-infinite bodies.

By numerical tests with different diffusion coefficients the following effects are found:

- the diffusion of Si from the fiber to the matrix in the samples without MgO dopant causes the increase of the average grain size on the rim of the fiber due to the decreasing concentration of SiO_2 on the rim.
- the diffusion of Mg from the matrix to the fiber causes the decrease of the average grain size on the rim of the fiber due to the increasing concentration of MgO on the rim.
- at high temperature (1400 C) the effect of the diffusion of Mg and Si on the grain size difference between the rim and the center of the fiber is larger;
- the combined diffusion of Mg and Si causes the decrease of the average grain size in full sample due to the faster diffusion of Mg. The effect of the Si diffusion slightly decreases.
- the GB diffusion coefficient of Mg is estimated to be larger than that of Si by 6 7 times that is in agreement with the data in the literature (see Table 4).

The developed model with estimated kinetic parameters allows us to make the predictions on the dopant concentration of the matrix and the heat treatment process parameters to fully or partially inhibit grain growth in ceramic composites.

7. Data availability

The datasets generated during and/or analysed during the current study are available from the corresponding author on reasonable request.

CRediT authorship contribution statement

Julia Kundin: Methodology, software, project administration, writing, validation, visualization. **Kamatchi Priya Ganesan:** software, writing draft and editing, visualization. **Renato S.M. Almeida, Hedieh Farhandi:** Data curation, experimental investigation, methodology, validation, writing draft and editing. **Kamen Tushtev:** project administration, conceptualization, supervision. **Kurosch Rezwan:** Funding acquisition, supervision.

Declaration of Competing Interest

The authors declare that they have no known competing financial interests or personal relationships that could have appeared to influence the work reported in this paper.

Acknowledgement

The authors would like to thank the German Research Foundation (DFG) for the financial support under grants KU 3122/3-1 and TU 364/

5-1.

References

[1] M. Schmücker, P. Mechnich, Improving the microstructural stability of NextelTM 610 alumina fibers embedded in a porous alumina matrix, J. Am. Ceramic Soc. 93 (2010) 1888 1890.
[2] M. Schmücker, P. Mechnich, Microstructural coarsening of NextelTM 610 fibers embedded in alumina-based matrices, J. Am. Ceramic Soc. 91 (2008) 1306 1308.
[3] M. Schmücker, F. Flucht, P. Mechnich, Degradation of oxide fibers by thermal overload and environmental effects, Mater. Sci. Eng. A 557 (2012) 10 16.
[4] R.S. Hay, G.E. Fair, T. Tidball, Fiber strength after grain growth in NextelTM 610 alumina fiber, J. Am. Ceram. Soc. 98 (2015) 1907 1914.
[5] H. Liu, C. Pei, J. Yang, Z. Yang, Influence of long-term thermal aging on the microstructural and tensile properties of all-oxide ceramic matrix composites, Ceram. Int. 46 (2020) 13989 13996.
[6] R.W. Rice, Relation of tensile strength-porosity effects in ceramics to porosity dependence of Young s modulus and fracture energy, porosity character and grain size, Mater. Sci. Eng. A. 112 (1989) 215 224.
[7] E. Volkmann, M.D. Barros, K. Tushtev, W. Pritzkow, D. Koch, J. Göring, et al., Influence of the matrix composition and the processing conditions on the grain size evolution of Nextel 610 fibers in ceramic matrix composites after heat treatment, Adv. Eng. Mater. 17 (2015) 610 614.
[8] I. Milas, B. Hinnemann, E.A. Carter, Structure of and ion segregation to an alumina grain boundary: implications for growth and creep, J. Mater. Res. 23 (5) (2008) 1494 1508.
[9] X.J. Zhang, G.J. Qiao, X. Zhang, Effect of Mg doping on the microstructure and properties of -Al2O3 transparent ceramics, Appl. Mech. Mater. 66 68 (2011) 1264 1269.
[10] R.H. Doremus, Diffusion in alumina, J. Appl. Phys. 100 (2006), 101301.
[11] J. Weissmüller, Alloy effects in nanostructures, Nanostruct. Mater. 3 (1 6) (1993) 261 272.
[12] R. Kirchheim, Grain coarsening inhibited by solute segregation, Acta Mater. 50 (2002) 413 419.
[13] F. Liu, R. Kirchheim, Nano-scale grain growth inhibited by reducing grain boundary energy through solute segregation, J. Cryst. Growth 264 (2004) 385 391.
[14] J.R. Trelewicz, C.A. Schuh, Grain boundary segregation and thermodynamically stable binary nanocrystalline alloys, Phys. Rev. B 79 (2009), 094112.
[15] M. Saber, H. Kotan, C.C. Koch, R.O. Scattergood, A predictive model for thermodynamic stability of grain size in nanocrystalline ternary alloys, J. Appl. Phys. 114 (2013), 103510.
[16] D. Mclean, Grain Boundaries in Metals, Oxford University Press, Oxford, 1957.
[17] D.S. Aidhy, Y. Zhang, W.J. Weber, Stabilizing nanocrystalline grains in ceramic-oxides, Phys. Chem. Chem. Phys. 15 (2013) 18915 18920.
[18] M.M. Gong, C.H. Chang, L.J. Wu, S. Dey, R.H.R. Castro, F. Liu, Modeling the grain growth kinetics of doped nearly fully dense nanocrystalline ceramics, Ceram. Int. 43 (2017) 6677 6683.
[19] M.M. Gong, R.H.R. Castro, F. Liu, Modeling the final sintering stage of doped ceramics: mutual interaction between grain growth and densification, J. Mater Sci. 53 (2018) 1680, 1616.
[20] S.J. Dillon, M.P. Harmer, Relating grain-boundary complexion to grain-boundary kinetics I: Calcia-doped alumina, J. Am. Ceram. Soc. 91 (2008) 2304 2313.
[21] S.J. Dillon, M.P. Harmer, Relating grain boundary complexion to grain boundary kinetics II: Silica-doped alumina, J. Am. Ceram. Soc. 91 (2008) 2314 2320.
[22] S.J. Dillon, M.P. Harmer, G.S. Rohrer, The relative energies of normally and abnormally growing grain boundaries in alumina displaying different complexions, J. Am. Ceram. Soc. 93 (2010) 1796 1802.
[23] M.P. Harmer, Interfacial kinetic engineering: how far have we come since Kingery s inaugural sosman address? J. Am. Ceram. Soc. 93 (2010) 301 317.
[24] G.S. Rohrer, Measuring and interpreting the structure of grain-boundary networks, J. Am. Ceram. Soc. 94 (2011) 633 646.
[25] C. Herzig, Y. Mishin, Grain boundary diffusion in metals, in: P. Heitjans, J. Kärger (Eds.), Diffusion in Condensed Matter, Springer, Berlin, Heidelberg, 2005.
[26] J.C. Fisher, Calculation of diffusion penetration curves for surface and grain boundary diffusion, J. Appl. Phys. 22 (1951) 74.
[27] R.T.P. Whipple, CXXXVIII. Concentration contours in grain boundary diffusion, Philos. Mag. 45 (1954) 1225.
[28] T. Suzuoka, Lattice and grain boundary diffusion in polycrystals, Trans. Jpn. Inst. Metals 2 (1961) 25.
[29] T. Suzuoka, Exact solutions of two ideal cases in grain boundary diffusion problem and the application to sectioning method, J. Phys. Soc. Jpn. 19 (1964) 839.
[30] A. Fukuura, Y. Oishi, Grain-boundary enhanced diffusion from instantaneous source in small-grain deep-penetration condition, J. Ceram. Soc. Jpn. 102 (1994) 897 901.
[31] G.H. Gilmer H.H. Farrell, Grain-boundary diffusion in thin films, I. The isolated grain boundary, J. Appl. Phys. 47 (1976) 3792.
[32] G.H. Gilmer H.H. Farrell, Grain-boundary diffusion in thin films, I. Multiple grain boundaries and surface diffusion, J. Appl. Phys. 47 (1976) 4373.
[33] W. Preis, W. Sitte, Grain boundary diffusion through thin films. Application to permeable surfaces, J. Appl. Phys. 79 (1996) 2986.
[34] J.C.M. Hwang, R.W. Balluffi, Measurement of grain-boundary diffusion at low temperatures by the surface accumulation method. I. Method and analysis, J. Appl. Phys. 50 (1979) 1339.
[35] B.S. Bokshtein, I.A. Magidson, I.L. Svetlov, On the diffusion in grains and grain boundaries, Phys. Met. Metallogr. 6 (1958) 81.
[36] W. Preis, W. Sitte, Modeling of fast diffusion along grain boundaries in oxide ceramics, Solid State Ionics 179 (2008) 765 770.
[37] I.V. Belova, G.E. Murch, Diffusion in nanocrystalline materials, J. Phys. Chem. Solids 64 (2003) 873.
[38] H.S. Levine, C.J. MacCallum, Grain boundary and lattice diffusion in polycrystalline bodies, J. Appl. Phys. 31 (1960) 595.
[39] Y. Chen, Ch. Schuh, Geometric considerations for diffusion in polycrystalline solids, J. Appl. Phys. 101 (2007), 063524.
[40] J. Kundin, R.S.M. Almeida, H. Salama, H. Farhandi, K. Tushtev, K. Rezwan, Phase-field simulation of abnormal anisotropic grain growth in polycrystalline ceramic fibers, Comput. Mater. Sci. 185 (2020) 109926, 109918.
[41] I. Steinbach, F. Pezzolla, A generalized field method for multiphase transformations using interface fields, Physica D 134 (1999) 385 393.
[42] I. Steinbach, X. Song, A. Hartmaier, Phase-field model with plastic flow for grain-growth in nanocrystalline material, Philos. Mag. 90 485 499.
[43] R.D. Kamachali, J. Hua, I. Steinbach, A. Hartmaier, Multiscale simulations on the grain growth process in nanostructured materials, Int. J. Mater. Res. 101 (11) (2010) 1332 1338.
[44] D.M. Wilson, D.C. Lueneburg, S.L. Lieder, High temperature properties of Nextel 610 and alumina-based nanocomposite fibers, Ceram. Eng. Sci. Proc. 14 (1993) 609 621.
[45] I. Manassidis, M.J. Gillan, Structure and energetics of alumina surfaces calculated from first principles, J. Am. Ceram. Soc. 77 (2) (1994) 335 338.
[46] P.R. Kenway, Calculated structures and energies of grain boundaries in a-Al2O3, J. Am. Ceram. Soc. 77 (2) (1994) 349 355.
[47] Y. Ji, J. Liu, M. Xu, K. Zeng, H. Jiang, C. Li, L. Yangc, Y. Chen, Evolution of crystal growth in MgO Al2O3 SiO2 glass ceramics, Cryst. Eng. Commun. 21 (2019) 1967 1973.
[48] M. Legall, A.M. Huntz, B. Lesage, J. Bernardini, Self-diffusion in -Al2O3 and growth rate of alumina scales formed by oxidation: effect of Y2O3 doping, J. Mater. Sci. 30 (1995) 201 211.